Soft Tissue Deformation Estimation Model Based on Spatial-Temporal Kriging for Needle Insertion Procedure

Linze Wang, Juntao Zhang, Mengxiao Zhao, and Dedong Gao(✉)

School of Mechanical Engineering, Qinghai University, Xining 810016, China
gaodd@zju.edu.cn

Abstract. The percutaneous surgery needs to know the soft tissue deformation in real time, but the existing prediction model cannot solve the problem. As a statistical interpolation method, kriging can effectively characterize the transformation of discrete point information into continuous facial information, so it can alleviate this problem. The tissue displacement of each identifying point in chronological order is obtained through the image processing of the experiment, and the spatial-temporal variogram function is selected to adapt the properties of soft tissue deformation in the needle insertion process. The permanent of spatial-temporal kriging is obtained based on the variogram function model of space and time, and the average error is 0.5 mm. The correlation of time and space is considered in spatial-temporal kriging, so the accuracy is higher. The kriging model compared with the data of another group of experiments, the average deviation is 0.2 mm. The feasibility and practicability of the model are verified.

Keywords: Soft tissue · Kriging · Spatial-temporal · Variogram

1 Introduction

Needle puncture surgery is a common treatment in medicine. Puncturing into the soft tissue reach the target to achieve diagnosis, treatment, sampling, stimulation and other purposes. Most of these puncture points are concentrated in organs, the common clinical application of tissue biopsy, local anesthesia, blood routine examination and others [1, 2]. In this process, the main causes of puncture error are: imaging equipment resolution limit, image coordinate deviation, target positioning error, human error, as well as the tissue deformation and needle deflection brought about by the target motion error [3–5]. In order to improve the accuracy of puncture and reduce the error, it is necessary to master the biological characteristics of soft tissue. The establishment of a soft tissue prediction model for real-time interaction between soft tissue and needle is of great significance for improving puncture accuracy and reducing puncture error [6].

Okamura et al. [7] put forward the empirical puncture force model, the puncture force is divided into three parts at first: stiffness forces, friction force and cutting. Stiffness forces is produced before the puncture of the membrane, and the friction force and

W. Li and D. Tang (Eds.): MOBILWARE 2020, LNICST 331, pp. 3–18, 2020.
https://doi.org/10.1007/978-3-030-62205-3_1

cutting are caused by the puncture of the membrane. The stiffness forces is fitting to a quadratic polynomial model, the friction force is represented by a modified Karnopp model, and the cutting power is a constant value. Podder et al. [8] considered the influencing factors of puncture force for the first time, and deduced a statistical model to estimate the maximum puncture force. The puncture force data were obtained by living experiments, and the statistical model of estimating maximum puncture force was verified based on individual parameters (such as body mass index, Gleason Fraction, pre-treatment, prostate volume) and specific treatment methods (such as puncture needle model, maximum puncture speed). Asadian [9] is based on the puncture force model proposed by Okamura, a modified LuGre model is used to simulate the acupuncture force, and the hysteresis characteristics of friction in the puncture process are analyzed and verified, and the dynamic process of friction is described in a complete description. Hing et al. [10] through linear elastic finite element analysis to develop the operating system to predict soft tissue deformation and puncture force. Misra [11] studied the mechanism of tissue fracture, the linear or nonlinear elasticity of tissue, and the effect of puncture needle deflection angle on the axial force and transverse force of needle. Using the contact and soft melt belt model, the finite element analysis is used to infer that the deflection angle of the smaller needle and the elasticity of the larger tissue will increase the stress of the needle tip. DiMaio and Sakcydean [12] explored the relationship between puncture force and tissue deformation for the first time. The axial force distribution of the needle is divided into two parts: the friction force between the needle and the tissue evenly distributed along the axial axis, and the peak power at the tip of the needle. Experiments show that the friction force of unit length increases with the increase of injection speed, and the peak at the tip of the needle is hardly changed with the speed of injection. Carra [13] studied the puncture force model of multi-layer tissue, in which the Hunt-Crossley model was used in the stiffness force of the membrane, and the use of the Dah friction model was adopted, and the cutting was a specific constant value corresponding to a particular tissue. In the whole puncture process, the puncture force is expressed by superposition principle and segmented function. Maurin [14] compared the puncture force between artificial and robotic operation during the biopsy of porcine living liver, and analyzed two types of puncture: one is direct puncture (other anatomical layers are removed), and the other is percutaneous puncture. Experiments show that the contribution of other anatomical layers to puncture force in percutaneous puncture is larger, and the puncture force of robot operation is relatively small. For the first time, Mahvash [15] analyzed the mechanical properties of acupuncture soft tissue by means of fracture mechanics, and the puncture membrane was described as the strain energy at the tip of the needle that exceeded the fracture toughness, prompting the crack to expand suddenly, and thus punctured the membrane. It is proved that increasing the feed speed of needle can reduce the peak of puncture force and tissue deformation. Sun Yinshan [16] of Harbin Institute of Technology and others put forward the generalized needle force model, which decomposes the stiffness forces into two parts using the Maurin model and the Simone model respectively. And put forward the robot assisted needle strategy: First, the needle into the liver moment, the robot automatically stops the needle, until the soft tissue back to relaxation, and then to halve the speed of the puncture; second, after the needle into the liver, if the puncture force exceeds a specific

threshold, the robot immediately stops the needle. Xuan Xinxiang [17] of Aeronautics and Astronautics and others based on the puncture force model proposed by Okamura, the modified Karnopp model was applied to the study of the mechanical properties of needle into corneal tissue. Gao Dedong [18], Tsinghua University, and others proposed a quasi-static finite element method for the analysis of soft tissue deformation, and a two-dimensional quasi-static finite element model of soft tissue deformation was created by using overlapping element method in ANSYS.

Researchers have carried out a lot of experimental research on acupuncture soft tissue, using experiments to observe the corresponding experimental phenomena (such as needle and tissue deformation, failure mechanism, etc.) and verify the accuracy of calculation or simulation results. Experimental platforms are often assisted by puncture robots, biological soft tissues (or imitation of soft tissues), imaging equipment, and control equipment. Okamura and Simone [19] using bovine liver as the experimental object, the deformation of liver tissue was measured by CT, and the stiffness of tissue, the resistance of the back membrane, the friction force and shear forces were measured, and the effect of needle deflection angle and needle diameter on puncture force was verified. Maurin et al. [14] took pig kidneys and liver as the research object, studied the change law of acupuncture into living tissue, and compared the difference between manual and robot. Considering the laboratory experimental conditions, it is not possible to scan the real biological tissue by CT and MRI, so many scholars use alternative materials with good transparent optical properties as the research object, and measure the deformation of the tissue and needle through high-speed cameras. DiMaio and Salcudean [20] used PVC material as the experimental object, implanted the regular calibration point in the gel, and then used high-speed camera to measure and analyze the tissue deformation. Jiang Shan et al. [21] have prepared transparent PVA materials with similarities in microstructure, mechanical properties and biological tissues, and have been used in puncture experimental research.

This paper is to study the deformation model of flexible needle puncture soft tissue. Based on the soft tissue puncture experiment, the identification object was set in the corresponding soft tissue (pork in this experiment), and the position coordinates of the flexible needle in the puncture soft tissue were recorded by B-ultrasound. Based on the image acquisition experiment, the image processing of flexible needle into soft tissue images was carried out to obtain the deformation of flexible needle and soft tissue in the process of injection. Combined with kriging model and soft tissue deformation are analyzed. In the previous soft tissue model, it was not good to solve the contradiction between accuracy and real-time, and often sacrificed another attribute for one attribute. In order to improve the contradiction between the two, this paper proposes a soft tissue prediction method based on spatiotemporal kriging method, which can effectively simplify the computation amount and improve the real-time performance of the model under certain precision. It can greatly simplify the calculation and improve the accuracy of the model under ensuring certain precision. In order to reduce the puncture error and improve the accuracy of the puncture to provide a reference.

2 Spatial-Temporal Kriging Model

2.1 Kriging Preliminaries

The idea of the kriging model was originally proposed by South African engineer Krige in his 1951 master's thesis and used this method to find a gold mine for the first time [22]. Then, in 1963, the method was systematized by the French mathematician Matheron, which formed a complete theory and model and named the method kriging [23], and was widely used in the field of ground statistical analysis. In the 1981, Professor Sacks et al. [24] once again promoted the kriging model, from the geological, hydrological, meteorological and other natural science fields to aerospace, automotive engineering and other fields of engineering science.

2.2 Spatial-Temporal Kriging Model

Commonly used kriging models include, ordinary Kriging (OK), simple Kriging (SK), and so on. They are widely used as an excellent interpolation algorithm in all walks of life, but they are spatial kriging models only can be depicted in a certain space at a specific time of the situation does not describe the process of continuous changes in space transactions. The puncture process of the puncture needle is a continuous process, and the doctor needs to know at all times what part of the needle is in the patient and the deformation of the soft tissue around the needle. The commonly used kriging model can no longer accurately describe the puncture process. And spatiotemporal Kriging not only takes into account the influence of space factors, but also adds the time factor, so that it can describe a continuous process, it can describe the deformation of soft tissue in the puncture process.

This paper extends on the basis of ordinary kriging and adds time parameters on the basis of ordinary Kriging.

$$Z^*(s_0, t_0) = \sum_{i=1}^{n} \lambda_i Z(s_i, t_i) \tag{1}$$

In the formula, $Z^*(s_0, t_0)$ is the estimate of space-time point, (s_0, t_0) and λ_i is the weighted coefficient of the adjacent observation value $Z(s_i, t_i)$. The kriging interpolation is based on the variogram function as the basic premise, in formula (1), the weighted coefficient λ_i is determined by the spatiotemporal variogram function. The calculation formula for the introduction of Lagrange coefficient μ to get parameter λ_i is:

$$\sum_{i=1}^{n} \lambda_i \gamma[(s_i, t_i) - (s_j, t_j)] + \mu = \gamma[(s_j, t_j) - (s_0, t_0)], \; j = 1, \ldots, n$$

$$\sum_{i=1}^{n} \lambda_i = 1$$

The weighted coefficient λ_i and Lagrange coefficient μ can be obtained from the above two-style.

2.3 Stationary Hypothesis

Hypothesis $Z(s,t)$ is a space-time stochastic process defined on $R^k \times T$, where R^k represents a k-dimensiona space, T represents time, an arbitrary sample point (s_i, t_i), $i = 1, \ldots, n$ position in space-time field, and h_s is a spatial distance between sample points and h_t is a time distance. If $Z(s,t)$ of the expectations are constant m, and the covariance function $Cov[Z(s,t), Z(s+h_s, t+h_t)]$ depends only on h_s and h_t independent of the specific position (s,t), then $Z(s,t)$ satisfies the second order stationary hypothesis, if the variance $Var[Z(s,t) - Z(s+h_s, t+h_t)]$ is limited and depends only on h_s and h_t, then $Z(s,t)$ satisfies the intrinsic hypothesis.

Therefore, when $Z(s,t)$ satisfies the second order stationary hypothesis or the intrinsic hypothesis, its covariance function can define

$$C(h_s, h_t) = Cov[Z(s+h_s, t+h_t) - Z(s,t)] \tag{2}$$

The variogram function is:

$$\gamma(h_s, h_t) = \frac{1}{2}E[Z(s+h_s, t+h_t) - Z(s,t)]^2 = \sigma^2 - C(s,t) \tag{3}$$

σ^2 is the variance of $Z(s,t)$.

2.4 Variogram

Variogram function is the most important step in constructing kriging model, and its function selection directly affects the interpolation accuracy of the model. The selection of the theoretical model of variogram function is mainly based on the relationship between distance and variation value, as well as the professional theory or experience to determine the appropriate theoretical model, but also can use scatter plot to speculate the appropriate theoretical model [25]. The area variables that are two points apart in space are recorded as $z(s_i + h_s, t_i + h_t)$ and $z(s_i.t_i)$ respectively, the spatial spacing is h_s, and the variogram function of $N(h_s, h_t)$ of the time interval h_t is [26]:

$$\gamma^*(h_s, h_t) = \frac{1}{2N(h_s, h_t)} \sum_{i=1}^{N(h_s,h_t)} [z(s_i + h_s, t_i + h_t) - z(s_i, t_i)]^2 \tag{4}$$

At present, the basic variogram function model is spherical model, exponential model, Gaussian model, power function model, pure nugget gold model and so on, and many new variation function models can be obtained by linear combination or multiplication of existing models [27, 28].

The parameters such as nugget, partial sill, sill and range of variogram function represent the spatial variation and correlation degree, and the strength of spatial correlation can be reflected by the partial sill/sill, if the greater the value, the stronger the spatial correlation. According to the theory of variogram function, the values of the two points in the same position should be equal, and with the increase of the distance (h), the numerical difference between the two points increases, until the sill value is tended, and the interval distance between the sampling points is range.

Due to the sampling error and spatial variation, two points are very close but there is also a nugget with a variogram function value of not zero. The discontinuity of the variogram function at the origin is called the Nugget Effect, and the data values of the adjacent two samples tend to vary greatly, the properties of the material change greatly in a very short distance. The nugget/sill is called the substrate effect, which is used to represent the variation characteristics between samples, and can also reflect the correlation, if the larger the value indicates more variation between samples caused by random factors. When the ratio of the nugget to the sill is $\leq$25%, the variable autocorrelation degree is strong, and if the ratio is between 25% and 75%, it is a medium autocorrelation level, and if the ratio is $\geq$75%, it is a weak autocorrelation level.

The soft tissue is mostly homogeneous material, so the nugget effect is weak, the nugget is very small so that the substrate effect is also very small, has a strong spatial correlation. Needle puncture surgery requires continuous, uniform and stable puncture process, in order to ensure the success of the puncture and reduce the patient's pain, so the time is also continuous and there is no variation, the nugget effect is weak and has a strong time correlation. The kriging interpolation method is based on the correlation of random variables in time and space.

3 Experimental Materials and Methods

3.1 Materials and Equipment

The choice of biological soft tissue material is a long about 25 cm, wide about 10 cm, thick about 5 cm of a shape of the regular pig leg meat. The meat in this area is evenly thick and easy to process into shape rules to facilitate the insertion of identifiers. Pork leg meat has typical soft tissue mechanical characteristics of anisotropy, and its mechanical properties in the direction of fiber and vertical fiber are different. Its mechanical properties can be obtained by SHPB experiment [29], in the case of strain rate of 0.02/S, the direction of the fiber is 121.00 $\pm$ 28.76 kPa, the ultimate strength is 63.73 $\pm$ 18.53 kPa, the damage strain is 0.934 $\pm$ 0.189; vertical fiber direction modulus is 47.60 $\pm$ 19.30 kPa, limit strength is 22.94 $\pm$ 3.63 kPa, damage strain is 1.077 $\pm$ 0.111 [30]. The identifier uses an iron nail with a diameter of about 2.3 mm and is arranged at a 1.5 cm distance interval.

The meat container is a custom U-type acrylic fixture, transparent colorless material easy to observe the placement of the meat, U-shaped adjustable shape can firmly fix the position of the meat. The needle is implemented by a three-axis puncture system, which can complete the movement of the XY plane and the rotation around the x axis, used to puncture the soft tissue of the needle and can adjust the posture and the position of the needle. The collection of pictures is completed by a medical B-ultrasound machine, the highest resolution of the B-ultrasound machine is 1 mm and provides two different probes of lower frequency convex and linear array, for experimental accuracy and image processing considerations, the test uses linear array probe to collect images.

The meat with the identifier is placed on the special fixture, and the puncture system is used to carry out the puncture experiment, and the B-ultrasound image is collected by the ultrasonic probe frame on the meat. Because of the limitation of the scanning width of the linear array ultrasonic probe, the internal situation of the whole organization cannot be observed at once, so the B-ultrasound image collected must be integrated in turn. The

stitched image is generally JPG format, which is not convenient for direct image processing. The general use of PS to convert its format to BMP format in image processing. Using Matlab to binarization it, improve the contrast of the image to reduce the difficulty of subsequent processing, corrosion removal of small, discrete, large area of noise in the image, expansion is that identifier image to amplify the recovery, noise reduction to remove the large noise spots, the marker marks the centroid of the remaining image and sends its coordinates to the specified location, and finally converts the coordinate units on the image from pixels to millimeters. The position of the identifier in the soft tissue can be obtained. The displacement of the identifier in the puncture process can be obtained by comparing the coordinate position of the image with different puncture depth.

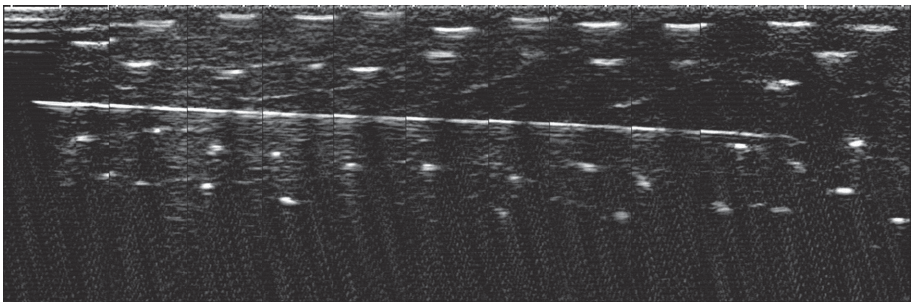

Fig. 1. B-ultrasonic image of needle into soft tissue.

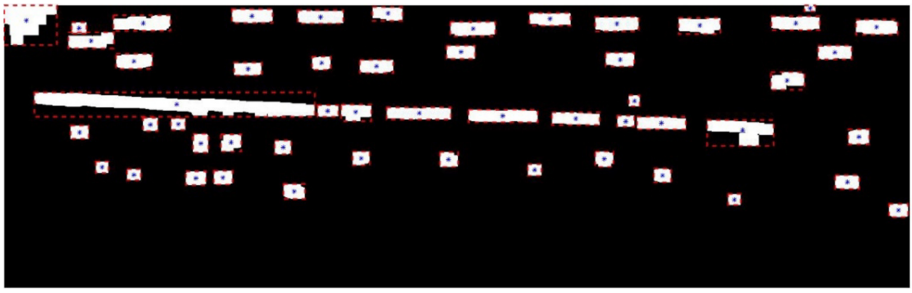

Fig. 2. Position of identifiers.

Figure 1 is a B-ultrasound image when the needle puncture is completed, the needle trajectory can be clearly seen, and because it is a flexible needle, deflection occurs in the soft tissue. The white spot area in the figure is the identifier in the tissue, because the B-ultrasound is ultrasonic reflection imaging, so in the distance from the B-ultrasound probe near the upper part, the image is clearer and because the distance is too close to a certain of lateral elongation. But because the centroid of the image is finally extracted from the image processing process, the lateral image elongation does not affect the

position of the centroid. So the distortion in the B-ultrasound image has less effect on the coordinates of the identified points. The image after Matlab processing is shown in Fig. 2, the middle slender image is connected to the trajectory of the needle, and the small white square around the needle is the identifiers after treatment. The black dots in the figure are the centroid of each image and the coordinates of the identifiers in the soft tissue. The position of the identifier in the soft tissue to be obtained through a series of steps in images processing. Due to various reasons such as device resolution limit and parameter setting in image processing, the identifier is not fully identified in the image processing at last. The displacement of 37 markers can be obtained by comparing it with the B-ultrasound image when the puncture is not carried out. Using the puncture needle progress as the time data, each puncture into the 1 cm to collect a B-ultrasound image. The final needle into the soft tissue about 16 cm, coupled with the image collected when not puncture can be processed to obtain a total of 17 sets of data, a total of 629 displacement data.

3.2 Spatial-Temporal Variogram Model

The spatial-temporal variogram function is extended by the spatial variogram function, and the time domain data has been added on the basis of the spatial domain. There are many differences between spatial domain and time domain. There exist many differences of parameters' properties in the spatial domain and time domain, such as the unit and the amount of data. Therefore, this paper uses the space-time model to fit the changes of soft tissue [27]. The structure is as follows:

$$C_{st}(h_s, h_t) = k_1 C_s(h_s) C_t(h_t) + k_2 C_s(h_s) + k_3 C_t(h_t) \tag{5}$$

$$\gamma_{st}(h_s, h_t) = (k_1 C_t(0) + k_2)\gamma_s(h_s) + (k_1 C_s(0) + k_3)\gamma_t(h_t) - k_1 \gamma_s(h_s)\gamma_t(h_t) \tag{6}$$

In the formula, C_{st} is spatiotemporal covariance, C_s is spatial covariance, C_t is time covariance, γ_{st} is spatiotemporal variogram function, γ_s is spatial variogram function, γ_t is time variogram function, $C_{st}(0, 0)$, $C_s(0)$, $C_t(0)$ are corresponding sill values respectively.

From the (5) formula,

$$C_{st}(0, 0) = k_1 C_s(0) C_t(0) + k_2 C_s(0) + k_3 C_t(0) \tag{7}$$

According to the derivation of reference [31], k_1, k_2 and k_3 can be solved by the following formula,

$$\begin{cases} k_1 = \dfrac{C_s(0) + C_t(0) - C_{st}(0, 0)}{C_s(0) C_t(0)} \\ k_2 = \dfrac{C_{st}(0, 0) - C_t(0)}{C_s(0)} \\ k_3 = \dfrac{C_{st}(0, 0) - C_s(0)}{C_t(0)} \end{cases} \tag{8}$$

The fitting data is the spatial data of 37 identifiers after image processing, and 17 groups of time data, and the variogram of the space domain is calculated by the curve fitting and the variogram of the time domain and fitted by the curve. As shown in Figs. 3 and 4.

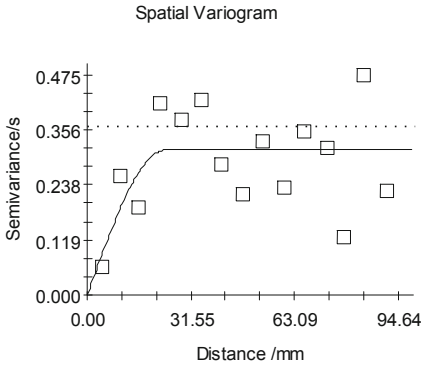

Fig. 3. Variogram of space.

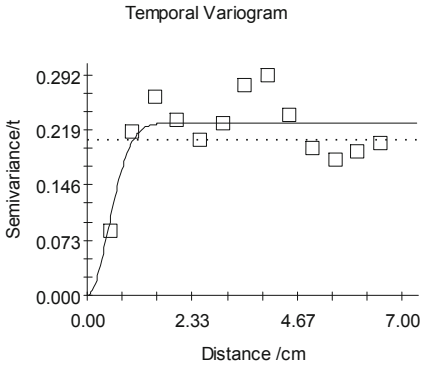

Fig. 4. Variogram of time.

The discrete block is the sample semi-variance, the curve is the corresponding fitting variogram function model, the relative spatial variogram function and the time variogramfunction are respectively,

$$\gamma(h_s) = 0.0001 + 0.3121(\frac{3}{2} \cdot \frac{h_s}{23.7} - \frac{1}{2} \cdot \frac{h_s^3}{23.7^3}) \tag{9}$$

$$\gamma(h_t) = 0.0001 + 0.2281(1 - e^{-\frac{h_t^2}{0.67^2}}) \tag{10}$$

Simultaneous formula (7) and formula (8), solvable $k_1 = 11.4448$,$k_2 = -1.6117$, $k_3 = -2.5731$, and formula (9) and formula (10) together with the formula (6) can get the spatiotemporal variogram function

$$\gamma_{st}(h_s, h_t) = (0.0001 + 0.3121(\frac{3}{2} \cdot \frac{h_s}{23.7} - \frac{1}{2} \cdot \frac{h_s^3}{23.7^3})) + 0.9999(0.0001 + 0.2281(1 - e^{-\frac{h_t^2}{0.67^2}}))$$
$$-11.4448(0.0001 + 0.3121(\frac{3}{2} \cdot \frac{h_s}{23.7} - \frac{1}{2} \cdot \frac{h_s^3}{23.7^3}))(0.0001 + 0.2281(1 - e^{-\frac{h_t^2}{0.67^2}}))$$

As shown in Fig. 5, the model fuses spatial variogram functions and temporal variogram functions, while preserving the characteristics of their trend changes.

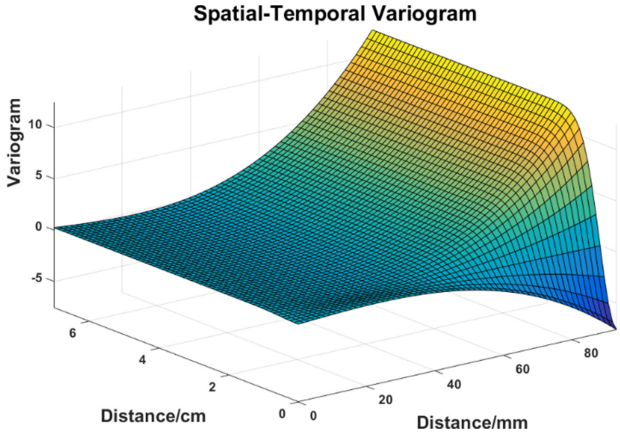

Fig. 5. Spatial-temporal variogram model.

The variation function will be obtained into the formula (1), the corresponding spatiotemporal kriging model is calculated. Unlike the spatial kriging model, adjacent sample points in space and time are involved in estimation when spatiotemporal interpolation. Therefore, the spatial-temporal kriging model is more granular and has continuity.

4 Results and Discussion

The spatiotemporal interpolation of the previously collected puncture data is carried out by using the variogram model described above, and the interpolation results are verified by cross-verification method. The interpolation results are in agreement with the actual situation, and the Fig. 6 is a prediction diagram of soft tissue deformation in different depths of puncture, in which the warmer the color represents the larger the displacement, and the colder the color represents the smaller the displacement. As can be seen from Fig. 6 that when the puncture needle first enters the soft tissue, the needle tip displacement is huge and the influence range is huge. This is because the needle tip has just stabbed into the soft tissue, the soft tissue is still glued to the needle tip area, resulting in the needle tip site displacement range beyond the normal impact range, in

the figure shows that the displacement into a wave forward reduction. When stabbed into 6 cm, the needle tip affects the range to restore to the normal range of influence. It is about an elliptical area of 2 cm in length and 1 cm in width, and the displacement starts from the center of the needle and gradually decreases from the middle to the sides. When puncture acupuncture into 12 cm, it can be obvious that the puncture needle has a downward offset phenomenon. The puncture needle is a beveled flexible puncture needle caused by the influence of the cutting force of the needle tip. In the last picture, the puncture needle was inserted into the 16 cm, almost completely inserted into the soft tissue, the needle body began to deflect downward, the impact range of the needle was extended to the sides by about 1.5 cm from the center of the needle. This is in line with the actual situation.

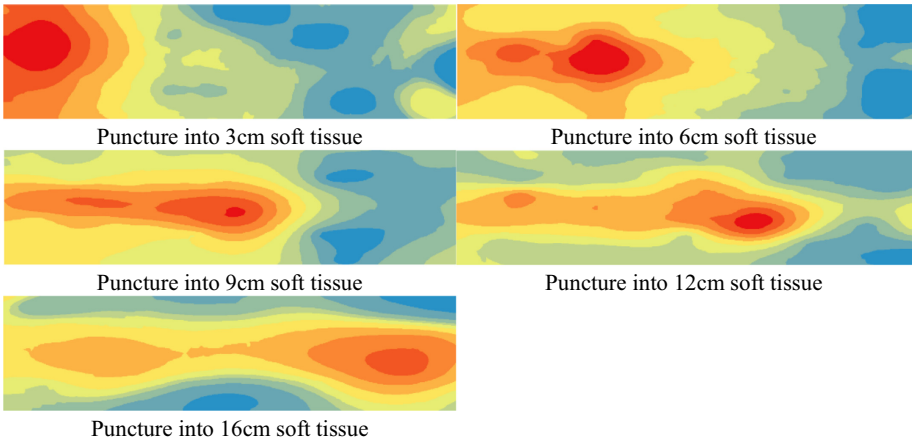

Fig. 6. Soft tissue deformation at different depths.

Cross-validation uses all data to estimate trends and autocorrelation models. It removes one data location at a time, and then predicts the associated data value. Compares the predicted value of the ellipsis position with the actual value,then repeat this procedure for the second point, and so on. Cross-validation compares the measured and predicted values for all points. After cross-validation is complete, if there are large errors in some data locations, those locations may be shelved as exceptions, and the trend model and autocorrelation model need to be redrafted. Cross-validation includes mean, root-mean-square, mean standardized, root-mean-square standardized, average standard error five evaluation indicators, in which the mean and root-mean-square are closer to zero, the better the average standard error and the mean standardized are as small as possible, the more the root-mean-square standardized is closer to 1 the better. Because the spatial interpolation scale range of this paper is very small, the average standard error and the root-mean-square error of each point are the main precision evaluation indexes, combined with the mean, the mean standardized error, the root-mean-square standardized error and so on. As you see from Table 1, the difference accuracy of spatiotemporal kriging is maintained at a high level. As the average standard error of the main measure, the value has a high precision level below 0.1.

Table 1. Analysis of interpolation accuracy.

Type	Depth	Mean	Root-Mean-Square	Mean Standardized	Root-Mean-Square Standardized	Average Standard Error
Spatiotemporal model	16 cm	0.0121	0.3387	0.0913	1.0658	0.4177
Space model	16 cm	−0.0152	0.4496	0.0691	1.3439	0.4529

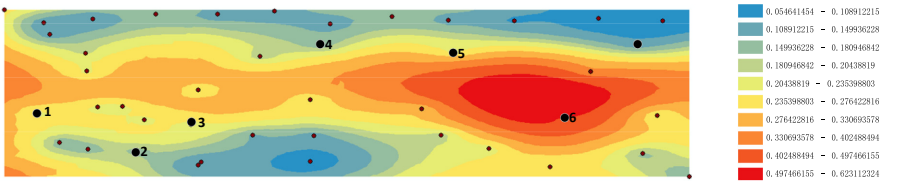

Fig. 7. Error distribution.

Most of the errors in Fig. 7 are below 0.5 mm, the error is small, and the interpolation accuracy is higher. The areas with large error are mainly distributed in the needle tip area and the needle body. Needle into the soft tissue, needle tip site deflection is the largest, in order to prevent the needle, hit the identifier to affect the measurement accuracy, so the needle tip area identifier setting is less. The needle is designed to allow enough area to allow the needle to pass through and thus less of the markers. The identifiers in these areas are sparse, the spatial information that can be interpolated is scarce, and the closer the kriging interpolation method is, the higher the accuracy, so the error of these sparse regions is larger.

The spatiotemporal Kriging model is compared with the simple space kriging model. Spatial kriging interpolation uses the data when puncture into 16 cm, regardless of the time factor, the comparison results are shown in Table 1. It is found that in the five criteria for measuring interpolation accuracy, the accuracy of the remaining four spatiotemporal models is higher than that of the spatial model, except for the mean standardized. This indicates that the spatial-temporal kriging model has higher accuracy and its interpolation results are closer to the actual value. Selecting 6 identification points for error comparison, the results are shown in Table 2, no matter where the space-time model accuracy is better than the spatial model accuracy, the error is reduced by an average of 20%. Identification points 1–5 are selected in areas where the Identification points are dense), spatial information is more abundant, so the accuracy of the improvement is not improved, about 10%–20%. And the identification point 6 is empty around, with very few identification points. At this time, the interpolation results of the spatial model have a large error, and the space-time model is adopted, considering the lack of spatial information supplemented by the information of the adjacent point of view, the interpolation accuracy has been significantly improved, and the far exceeding the average value has been increased by 34%.

Table 2. Comparison the accuracy of spatial-temporal kriging and spatial kriging.

Number	Spatial-temporal kriging	Spatial kriging	Improvement of accuracy (%)
1	0.2194	0.2832	22.5501
2	0.1672	0.1906	12.2954
3	0.2104	0.2624	19.8415
4	0.1556	0.1967	20.9028
5	0.2201	0.2541	13.3873
6	0.4769	0.7242	34.1481

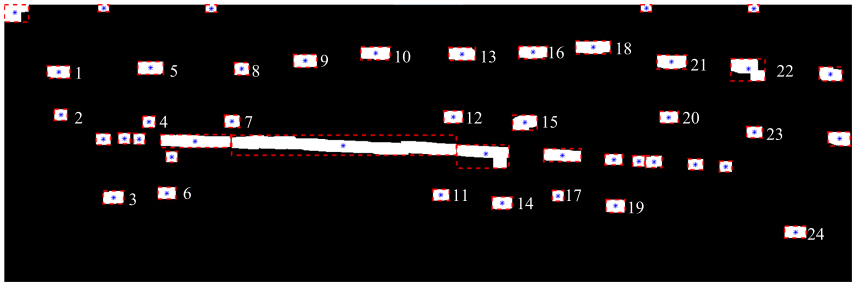

Fig. 8. The Identifier coordinates of the test.

In order to verify the feasibility of the model, another set of test data is selected for verification. Select the experimental data for the puncture 16 cm data, after image processing and other steps, the final results as shown in Fig. 8. From the Fig. 8, it can be seen that the middle bending part is still the needle, around the spread of the white square as the identifier, and 24 points are selected as the verification point. These points are distributed on both sides of the needle body and are covered with the entire image. The 2,4,7,12,15 and other points are close to the needle body, and the 1,5,8,9 points is far away from the needle body and runs through the image, while the 3,6,11 and other points are distributed under the needle body. The selected points are distributed across parts of the image and are far closer to the distance of the needle body. The above results analysis can verify that the spatiotemporal Kriging model has predictive power for each location.

The data predicted by the spatiotemporal kriging model are compared with the data of the verification test itself and plotted into a scatter plot, as shown in Fig. 9. The maximum deviation occurs at the 12th verification point is 0.64 mm, the minimum deviation is 0.01 mm at the 1th verification point, and the average deviation is 0.2 mm. It is proved that the interaction model of needle and soft tissue constructed by spatiotemporal kriging interpolation method is fully satisfied with the requirement of millimeter grade accuracy of needle puncture operation, and the accuracy is higher to meet the needs of operation.

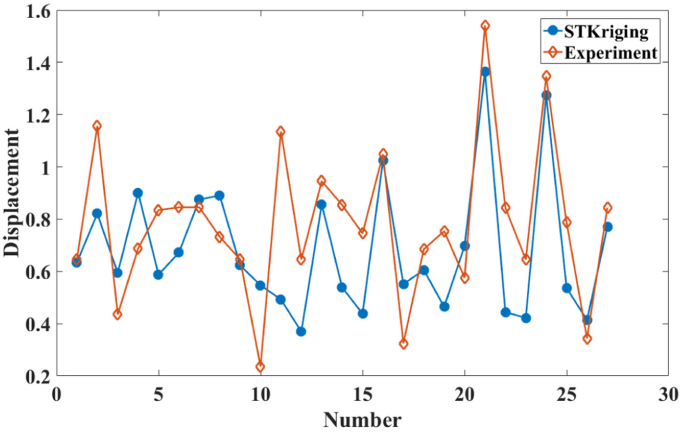

Fig. 9. Comparison the identification displacement of spatial-temporal kriging model and test.

5 Conclusions and Future Work

The needles puncture soft tissue is a continuous process. The displacement of soft tissue in the puncture process is not only strongly correlated in space, but also closely related to the depth (time). In the estimation, therefore, considering the measurement value near the point in time can effectively improve the interpolation accuracy, and the process of needles puncture can be restored as much as possible. The suitable variogram model is an important foundation of high precision kriging interpolation, and the this paper using kriging model product by spatiotemporal variogram model which combines spatial and time model, so that it retains the changing trends of each other. Experimental results show that the model has high accuracy, which is better than the simple spatial kriging interpolation, both in the description of the puncture process and the accuracy of the model, and also realizes the prediction in the future [31]. However, the time factor added to the model, the amount of data in the experiment is greatly increased, which also increases the calculation and the difficulty of the variogram function, so it is very important for the spatiotemporal model to choose the sampling frequency and data processing method.

Kriging model compares with the traditional soft tissue model, such as mass-spring model and finite element model, the advantage of spatiotemporal kriging model is that it can greatly simplify the calculation under the condition of ensuring high precision, so the real-time performance is greatly increased. The spatiotemporal variogram model used in this paper extends the time parameters on the basis of ordinary kriging interpolation, but in the actual process, many factors can affect the deformation of soft tissue, such as different soft tissues have different parameters. In the subsequent research, more factors of soft tissue, such as elastic modulus, will be considered to optimize the variogram function and improve the spatiotemporal kriging accuracy.

References

1. Rizun, P.R., Mcbeth, P.B., Louw, D.F.: Robot- assisted neu- rosurgery. Surg. Innov. **11**, 99–106 (2004)
2. Zivanovic, A., Davies, B.L.: A robotic system for blood sampling. IEEE Trans. Inf. Technol. Biomed. **4**(1), 8–14 (2000)
3. Carr, J.J., Hemler, P.F., Halford, P.W., Freimanis, R.I., Choplin, R.H., Chen, M.Y.: Stereotactic localization of breast lesions: how it works and methods to improve accuracy. Radiographics: a review publication of the Radiological Society of North America **21**(2), 463–473 (2001)
4. Hussain, H.K., Kingston, J.E., Domizio, P., Norton, A.J., Reznek, R.H.: Imaging-guided core biopsy for the diagnosis of malignant tumors in pediatric patients. Am. J. Roentgenol. **176**(1), 43–47 (2001)
5. Roberson, P.L., Narayana, V., McShan, D.L., Winfield, R.J., McLaughlin, P.W.: Source placement error for permanent implant of the prostate. Med. Phys. **24**(2), 251–257 (1997)
6. Gao, D.: Tissue deformation mechanism and dynamic path planning for flexible needle into soft tissue. Zhejiang University (2017)
7. Okamura, A.M., Simone, C., O'Leary, M.D.: Force modeling for needle insertion into soft tissue. IEEE Trans. Bio-Med. Eng. **51**(10), 1707–1716 (2004)
8. Podder, T.K., Sherman, J., Clark, D.P.: Evaluation of robotic needle insertion in conjunction with in vivo manual insertion in the operating room. In: IEEE International Workshop on Robot & Human Interactive Communication (2005)
9. Asadian, A., Kermani, M.R., Patel, R.V.: A compact dynamic force model for needle-tissue interaction. In: International Conference of the IEEE Engineering in Medicine & Biology (2010)
10. Hing, J.T., Brooks, A.D., Desa,i J.P.: Reality-Based Estimation of Needle and Soft-Tissue Interaction for Accurate Haptic Feedback in Prostate Brachytherapy Simulation. In: Thrun, S., Brooks, R., Durrant-Whyte, H., (eds) Robotics Research. Springer Tracts in Advanced Robotics, vol 28. Springer, Berlin, Heidelberg (2007) https://doi.org/10.1007/978-3-540-48113-3_4
11. Misra, S., Reed, K.B., Schafer, B.W., Ramesh, K.T., Okamura, A.M.: Mechanics of flexible needles robotically steered through soft tissue. Int. J. Robot. Res. **29**, 1640–1660 (2010)
12. Dimaio, S.P., Salcudean, S.E.: Needle insertion modelling and simulation. In: IEEE International Conference on Robotics & Automation (2002)
13. Carra, A., Avila-Vilchis, J.C.: Needle insertion modeling through several tissue layers. In: International Asia Conference on Informatics in Control (2010)
14. Maurin, B., et al.: In: Vivo Study of Forces During Needle Insertions (2015)
15. Mahvash, M.: Haptic rendering of cutting. a fracture mechanics approach, Hapticse, Electron. J. Haptics Res. **2**, 1–12 (2011)
16. Yinshan, S., Dongmei, W., Zhijiang, D., Lining, S.: Modeling of needle insertion force in porcine livers for studying needle insertion strategies of robot-assisted percutaneous surgery. Chinese High Technol. Lett. **21**, 948–953 (2011)
17. Xuan, X., Yang, Y., Wang, Z., Deng, S., Liu, X.: Mechanical model of suture acupuncture into corneal tissue. Chinese High Technol. Lett. **19**, 951–956 (2009)
18. Dedong, G., Yipeng, G., Haojun, Z.: A finite element approach for simulating soft tissue deformation during needle insertion. J. Comput. Aided Des. Comput. Graph. **21**, 1601–1605 (2009)
19. O'leary, M.D., Simone, C., Washio, T.: Robotic needle insertion: effects of friction and needle geometry. In: IEEE International Conference on Robotics & Automation (2003)
20. Dimaio, S.P., Salcudean, S.E.: Needle steering and motion planning in soft tissue. IEEE Trans. Biomed. Eng. **52**, 965–974 (2005)

21. Jiang, S., Liu, S., Feng, W.: PVA hydrogel properties for biomedical application. J Mech Behave Biomed. Mater. **4**(7), 1228–1233 (2011)
22. Krige, D.G.: A statistical approach to some basic mine valuation problems on the witwatersrand. J. Mech. Behav. Biomed. Mater. **4**, 18 (1953)
23. Matheron, G.: Principles of geostatistics. Econ. Geol. **58**, 1246–1266 (1963)
24. Santner, T.J., Williams, B.J., Notz, W.I.: Design and analysis of computer experiments. Asta Adv. Stat. Anal. **4**, 409–423 (1989)
25. Clark, D.S.: Adjudication to administration: a statistical analysis of federal district courts in the twentieth century. S. Cal. L. Rev. **55**, 65 (1981)
26. Webster, R.: Quantitative spatial analysis of soil in the field. Adv. Soil Sci. **3**, 537–542 (1985)
27. Cesare, L.D., Myers, D.E., Posa, D.: Estimating and modeling space–time correlation structures. Stat. Probab. Lett. **51**, 9–14 (2001)
28. Ma, C.: Families of spatio-temporal stationary covariance modes. J. Stat. Plan. Inference **116**, 489–501 (2003)
29. Wang, B., Zheng, Y., Hu, S.: Dynamic tensile properties of porcine hind leg muscles. Expl. Shocks **30**, 449–455 (2010)
30. Wang, B.: Research on dynamic mechanical properties of soft muscle tissue. University of Science and Technology of China (2010)
31. Cesare, D.L., Myers, E.D., Posa, D.: Product-sum covariance for space -time modeling, An environmental application. Environmetrics **12**, 11–23 (2001)